Analysis of Vibrational Modes of the P_4 Molecule Through Hyperspherical Variants of the Local Orthogonal Coordinates: The Limit of Dissociation in Dimers

MIRCO RAGNI,[1] FREDERICO V. PRUDENTE,[1] ANA C. P. BITENCOURT,[2] PATRICIA R. P. BARRETO[3]

[1]*Instítuto de Física, Universidade Federal da Bahia (UFBA), Salvador, Bahia, Brazil*
[2]*Centro de Formação de Professores, Universidade Federal do Recôncavo da Bahia (UFRB), Amargosa, Bahia, Brazil*
[3]*Laboratorio Associado de Plasma, Instituto Nacional de Pesquisas Espaciais, São José dos Campos, São Paulo, Brazil*

Received 27 February 2010; accepted 26 March 2010
Published online 24 August 2010 in Wiley Online Library (wileyonlinelibrary.com).
DOI 10.1002/qua.22763

ABSTRACT: In this work, we discuss the representation in different orthogonal coordinates sets of highly symmetric P_4 molecule whose equilibrium configuration is tetrahedral. For this purpose, the H (or diatom–diatom) and Wigner orthogonal representations are used to study the singlet (ground) electronic state of the title molecule, whereas the V (or diatom–satellites) scheme is used in the triplet electronic state analysis. The equilibrium geometries and the respective electronic energies of $P_n, n = 1, \ldots, 4$, are determined using the coupled cluster and DFT methodologies. Moreover, the vibrational harmonic modes and the minimum energy path of the P_4 dissociation in P_2 dimers are calculated within DFT procedure. From these calculations, the diatom–diatom and Wigner vectors are used to analyze the behavior of vibrational modes, and the possible fragmentation channels ($P_4 \rightarrow 2P_2, P_3 + P, P_2 + 2P, 4P$) are discussed. The presented results are compared, when available, with previous theoretical and experimental ones.

Key words: orthogonal local coordinates; orthogonal Hamiltonian; cluster of phosphours; hyperspherical coordinates

Correspondence to: M. Ragni; e-mail: mirco.ragni@gmail.it
Contract grant sponsors: CNPq, FAPESB.

1. Introduction

The choice of appropriated coordinate sets to describe a molecular system is a strategy that simplifies the study of the intermolecular dynamics. The local orthogonal coordinates have the property of expressing the relative kinetic energy of the system in diagonal form, without cross derivatives in the Schrödinger equation [1, 2]. We are looking for sets of coordinates that are useful to represent the modes of vibration near the equilibrium configuration and to simplify the representation of the potential energy surface [3]. In this work, we are interested in describe the systems with tetrahedral equilibrium configuration as the P_4 molecule.

There are many theoretical [4–6] and experimental [7, 8] studies for P_4 molecule. In literature, theoretical studies present structural and energetic properties of P_n clusters (closed-shell clusters up to $n = 18$) [9, 10] and reactive processes involving P_4 [11, 12]. The highly symmetric P_4 molecule has a tetrahedral equilibrium configuration [6] in the singlet ground state and belongs to the tetrahedral Td symmetry group. In this case, a good choice of the six internal coordinates needs to be related to the irreducible representations of the Td point group. On the other hand, the triplet P_4, which is formally obtained by exciting one electron of the singlet P_4 from a bond orbital to an antibond one, belongs to the C_{2v} symmetry. Then, a good choice of the six internal coordinates needs to be related to the irreducible representations of this point group.

Our goal is to exploit advantages coming from the use of different schemes of local orthogonal coordinates [13–16] to analyze the vibrational modes of P_4 molecule and to describe the possible fragmentation channels. We use diatom–diatom (or H) [3, 17, 18], Wigner (or W) [2], and diatom–satellites (or V) [19] orthogonal representations to study the P_4 system. The so-called H scheme is the most divulged in literature, and it is used to study the bound-state problems [16], large amplitude motions [20], dimmers [21, 22], and reaction processes [23, 24]. The simplicity of this scheme will be exploited here to describe vibrational modes and fragmentation channels of the singlet P_4. This scheme of orthogonal coordinates then will be compared with the W one that has a property of the correct representation of the tetrahedral symmetries. The triplet state, instead, could be described with the V scheme of coordinates, which are related to the irreducible representation of the C_{2v} group.

From these local orthogonal coordinates, asymmetric hyperspherical variants can be introduced following the Aquilanti and Cavalli procedure [25]. These parameterizations define a (internal) six-dimensional space described by the hyperradius and five hyperangles. The hyperspherical variables behave like the normal modes close to the minimum of the potential energy surface [26]. These internal coordinates could also permit a global representation of the potential energy surface simplifying the intramolecular dynamics.

Structural and energetic properties are calculated by quantum chemistry method for P_n, $n = 1, \ldots, 4$. In particular, we have chosen to use the CCSD(T) method and the aug-cc-pVQZ basis set following a precedent work [6]. Moreover, we have also used the B3LYP procedure in the calculations to reduce the computational time when the normal modes of vibration and the minimum energy path of the P_4 dissociation are evaluated. The results will be discussed with the purpose of elucidating the features of the internal modes of the P_4 molecule and to describe the reactive channels in terms of hyperspherical coordinates.

This article is structured as follows. In section 2 the H, W, and V local orthogonal coordinates are discussed, and the hyperspherical variants are introduced. Results and discussions are presented in section 3. Section 4 reports conclusions and some remarks.

2. Local Orthogonal Coordinates and Hyperspherical Variants

The local orthogonal coordinates for four particles used to describe the P_4 molecule are introduced in this section. Specifically, Figure 1 shows the H and W vectors, whereas the V vectors are displayed in Figure 2. A general feature of the local orthogonal coordinates is the separation between the center of mass motion and the relative one by introduction of the center of mass vector and the other three relative ones [1, 2, 13]. The center of mass vector can be neglected when no external force acts on the system. The remaining three vectors describe the internal motion (six coordinates) and the external rotation (the three Euler angles, for instance). Following the procedure adopted in Ref. [25], we define the asymmetric hyperspherical coordinates of the H, W, and V schemes.

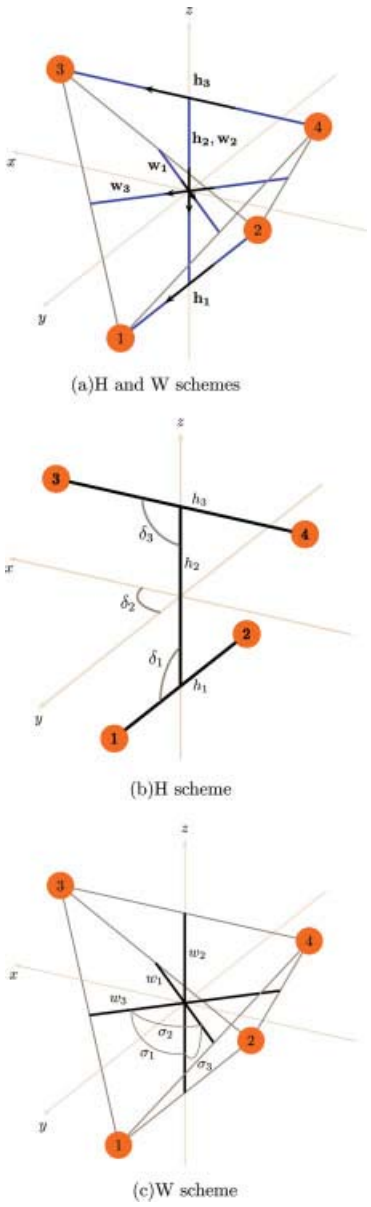

FIGURE 1. (a) The diatom–diatom (H) and Wigner (W) schemes of vectors, used to describe the molecule of P_4, are depicted superposed. (b) The coordinates of the H scheme are shown. Starting from the vectors $\mathbf{h}_1$, $\mathbf{h}_2$, and $\mathbf{h}_3$, Eq. (2), the six internal coordinates are defined as three distances h_1, h_2, and h_3 that are related to the modules of the vectors, two angles δ_1 and δ_3, and the dihedral angle δ_2. Note that δ_2 is not the angle between the x and y axis. (c) The coordinates of Wigner scheme defined in Section 2.1 are shown. The internal coordinates built up starting from this scheme are the three distances w_1, w_2, and w_3 related to the modules of the vectors and the three angles σ_1, σ_2, and σ_3 between them, all depicted in figure. [Color figure can be viewed in the online issue, which is available at wileyonlinelibrary.com.]

2.1. DIATOM–DIATOM SCHEME

The H vectors [2, 3, 27] [see Figs. 1(a) and (b)] can be obtained from the laboratory position vectors using the kinematic rotation matrices procedure [13, 28]. Their mass-scaled form is given by

$$\mathbf{h}_1 = \sqrt{\frac{m_1 m_2}{m M_{12}}}(\mathbf{r}_1 - \mathbf{r}_2),$$
$$\mathbf{h}_2 = \sqrt{\frac{M_{34}}{M_{12}}}\left[\frac{m_1\mathbf{r}_1 + m_2\mathbf{r}_2}{m}\right] - \sqrt{\frac{M_{12}}{M_{34}}}\left[\frac{m_3\mathbf{r}_3 + m_l\mathbf{r}_4}{m}\right],$$
$$\mathbf{h}_3 = \sqrt{\frac{m_3 m_4}{m M_{34}}}(\mathbf{r}_3 - \mathbf{r}_4), \tag{1}$$

where m_i and $\mathbf{r}_i$ ($i = 1,2,3,4$) are the mass and the position vector of the ith particle, respectively, M_{ij} is the sum of the masses of the i and j particles and m is the total mass of the system. When the four particles have identical masses, the H vectors can be written as

$$\mathbf{h}_1 = \frac{1}{\sqrt{2}}\frac{\mathbf{r}_1 - \mathbf{r}_2}{2},$$
$$\mathbf{h}_2 = \frac{\mathbf{r}_1 + \mathbf{r}_2 - \mathbf{r}_3 - \mathbf{r}_4}{4},$$

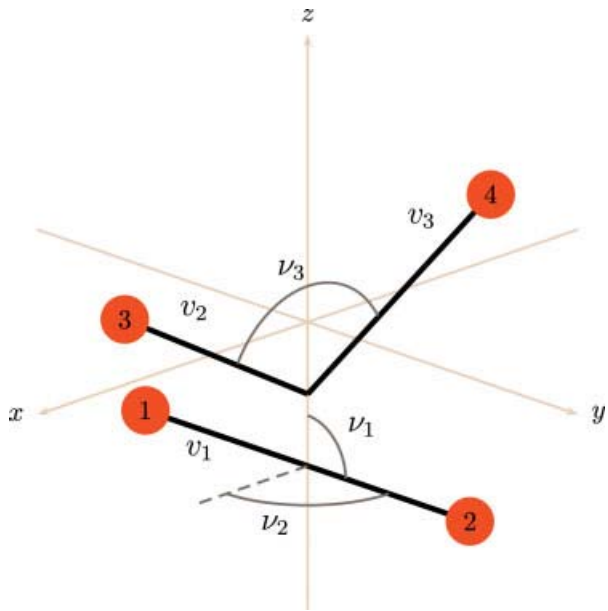

FIGURE 2. Diatom–satellites (V) vectors and the six internal coordinates used to describe the modes of vibration and the dissociative channels of the triplet P_4. [Color figure can be viewed in the online issue, which is available at wileyonlinelibrary.com.]

$$\mathbf{h}_3 = \frac{1}{\sqrt{2}}\frac{\mathbf{r}_3 - \mathbf{r}_4}{2}. \tag{2}$$

In this scheme, the kinetic energy operator is given by

$$\hat{T}(\mathbf{h}) = -\frac{\hbar^2}{2m}\sum_{i=1}^{3}\nabla^2_{\mathbf{h}_i}. \tag{3}$$

The relationships of the H vectors with the interparticle ones are given by:

$$\begin{aligned}
\mathbf{r}_{12} &= 2\sqrt{2}\mathbf{h}_1,\\
\mathbf{r}_{13} &= \sqrt{2}\mathbf{h}_1 + 2\mathbf{h}_2 - \sqrt{2}\mathbf{h}_3,\\
\mathbf{r}_{14} &= \sqrt{2}\mathbf{h}_1 + 2\mathbf{h}_2 + \sqrt{2}\mathbf{h}_3,\\
\mathbf{r}_{23} &= -\sqrt{2}\mathbf{h}_1 + 2\mathbf{h}_2 - \sqrt{2}\mathbf{h}_3,\\
\mathbf{r}_{24} &= -\sqrt{2}\mathbf{h}_1 + 2\mathbf{h}_2 + \sqrt{2}\mathbf{h}_3,\\
\mathbf{r}_{34} &= 2\sqrt{2}\mathbf{h}_3,
\end{aligned} \tag{4}$$

where the distance between the i and j particles is defined as $r_{ij} = |\mathbf{r}_{ij}|$. Moreover, the distances between particles 1 and 2 (h_1), particles 3 and 4 (h_3), and the center of mass of diatoms 12 and 34 (h_2) are the following [see Fig. 1(b)]:

$$\begin{aligned}
h_1 &= 2\sqrt{2}|\mathbf{h}_1|,\\
h_3 &= 2\sqrt{2}|\mathbf{h}_3|,\\
h_2 &= 4|\mathbf{h}_2|.
\end{aligned} \tag{5}$$

It is interesting to define also the coordinates δ_1, angle between the $\mathbf{h}_1$ and $\mathbf{h}_2$ vectors, δ_3, angle between the $\mathbf{h}_2$ and $\mathbf{h}_3$ vectors, and δ_2, the dihedral angle between the $\mathbf{h}_1$ and $\mathbf{h}_3$ vectors. These coordinates, together with h_1, h_3, and h_2, represent a good internal coordinate set to describe the geometrical parameters [13].

A particular hyperspherical parametrization [25, 26] obtained from the modules of these vectors allows to introduce another type of internal coordinates:

$$\begin{aligned}
\rho &= \sqrt{|\mathbf{h}_1|^2 + |\mathbf{h}_2|^2 + |\mathbf{h}_3|^2},\\
\chi_1 &= \arctan\frac{|\mathbf{h}_1|}{|\mathbf{h}_3|},\\
\chi_2 &= \arctan\frac{|\mathbf{h}_2|}{\sqrt{|\mathbf{h}_1|^2 + |\mathbf{h}_3|^2}},
\end{aligned} \tag{6}$$

where ρ is the hyperradius, and the angular part is described by five hyperangles: χ_1, χ_2, δ_1, δ_2, and δ_3. These variables define a six-dimensional hyperspherical space, and they can be useful to describe the modes of vibration and to represent the potential energy surfaces for internuclear dynamics, as it will be discussed in Section 3.

2.2. WIGNER SCHEME

The W scheme [see Figs. 1(a) and (c)] is a symmetric orthogonal representation credited to Wigner [1], and it is given in terms of three vectors for the case of four particles of the same mass (one alternative formulation of Wigner scheme to nonequal masses is discussed in appendix). These vectors are built up as those three vectors that join the centers of mass of each of the three couples of particles of the instantaneous tetrahedral configuration. They can be obtained by applying the kinematic rotation matrix

$$\mathbf{K} = \begin{pmatrix} \frac{1}{\sqrt{2}} & 0 & \frac{1}{\sqrt{2}} \\ 0 & 1 & 0 \\ -\frac{1}{\sqrt{2}} & 0 & \frac{1}{\sqrt{2}} \end{pmatrix} \tag{7}$$

into the matrix representation of the H vectors for identical masses. The resulting mass-scaled vectors are

$$\begin{aligned}
\mathbf{w}_1 &= \frac{\mathbf{r}_1 - \mathbf{r}_2 - \mathbf{r}_3 + \mathbf{r}_4}{4},\\
\mathbf{w}_2 &= \frac{\mathbf{r}_1 + \mathbf{r}_2 - \mathbf{r}_3 - \mathbf{r}_4}{4},\\
\mathbf{w}_3 &= \frac{\mathbf{r}_1 - \mathbf{r}_2 + \mathbf{r}_3 - \mathbf{r}_4}{4},
\end{aligned} \tag{8}$$

where $\mathbf{r}_i$ ($i = 1, 2, 3, 4$) is the position vector of the ith particle. The kinetic energy operator in the W scheme is given by

$$\hat{T}(\mathbf{w}) = -\frac{\hbar^2}{2m}\sum_{i=1}^{3}\nabla^2_{\mathbf{w}_i}. \tag{9}$$

The internal parameters that define the molecular geometry shown in Figure 1(c) are derived from Wigner vectors. In particular, the three distances are the following:

$$w_j = 4|\mathbf{w}_j| \quad \text{with} \quad j = 1, 2, 3, \tag{10}$$

while the three angles are: σ_1, between the $\mathbf{w}_2$ and $\mathbf{w}_3$ vectors, σ_2, between the $\mathbf{w}_1$ and $\mathbf{w}_3$ vectors, and σ_3,

between the $\mathbf{w}_1$ and $\mathbf{w}_2$ vectors. The relationships of W vectors with the interparticle ones are given by

$$\begin{aligned}
\mathbf{r}_{12} &= 2(\mathbf{w}_1 + \mathbf{w}_3),\\
\mathbf{r}_{13} &= 2(\mathbf{w}_1 + \mathbf{w}_2),\\
\mathbf{r}_{14} &= 2(\mathbf{w}_2 + \mathbf{w}_3),\\
\mathbf{r}_{23} &= 2(\mathbf{w}_2 - \mathbf{w}_3),\\
\mathbf{r}_{24} &= 2(\mathbf{w}_2 - \mathbf{w}_1),\\
\mathbf{r}_{34} &= 2(\mathbf{w}_3 - \mathbf{w}_1),
\end{aligned} \tag{11}$$

and $r_{ij} = |\mathbf{r}_{ij}|$.

A particular hyperspherical parametrization from the modules of these vectors allows to introduce another type of internal parameters that are defined by:

$$\begin{aligned}
\rho &= \sqrt{|\mathbf{w}_1|^2 + |\mathbf{w}_2|^2 + |\mathbf{w}_3|^2},\\
\chi_3 &= \arctan \frac{|\mathbf{w}_1|}{|\mathbf{w}_3|},\\
\chi_4 &= \arctan \frac{|\mathbf{w}_2|}{\sqrt{|\mathbf{w}_1|^2 + |\mathbf{w}_3|^2}}.
\end{aligned} \tag{12}$$

As it can be understood from the kinematic rotation matrix that relates the Wigner scheme to the H one, Eq. (7), $\mathbf{w}_2 = \mathbf{h}_2$ and $|\mathbf{w}_1|^2 + |\mathbf{w}_3|^2 = |\mathbf{h}_1|^2 + |\mathbf{h}_3|^2$. Consequently, the hyperangles χ_2 (H scheme) and χ_4 (W scheme) are equal. Equivalently to the internal coordinates of the H scheme introduced at the end of the previous subsection, the coordinates ρ, χ_3, χ_4, σ_1, σ_2, and σ_3 can be used to describe the modes of vibration. The symmetries of the Wigner scheme suggest that the interaction potential of tetrahedral molecules, like the P_4, is substantially factorized near the equilibrium configuration, if represented in terms of these coordinates.

The H and W schemes are used to analyze the singlet ground electronic state of P_4 in Section 3.

2.3. DIATOM–SATELLITES SCHEME

The last scheme, the so-called V one [13] (see Fig. 2), is defined from the position vectors as follows,

$$\begin{aligned}
\mathbf{v_1} &= \frac{\mathbf{r}_1 - \mathbf{r}_2}{2\sqrt{2}},\\
\mathbf{v_2} &= \frac{1}{4\sqrt{2}}(\mathbf{r}_1 + \mathbf{r}_2) + \frac{1}{4}\left(1 - \frac{1}{\sqrt{2}}\right)\mathbf{r}_4 - \frac{1}{4}\left(1 + \frac{1}{\sqrt{2}}\right)\mathbf{r}_3,\\
\mathbf{v_3} &= \frac{1}{4\sqrt{2}}(\mathbf{r}_1 + \mathbf{r}_2) + \frac{1}{4}\left(1 - \frac{1}{\sqrt{2}}\right)\mathbf{r}_3 - \frac{1}{4}\left(1 + \frac{1}{\sqrt{2}}\right)\mathbf{r}_4,
\end{aligned} \tag{13}$$

for the case of four equal masses. As it was considered previously, the vector of the center of mass has been neglected. Formally, the V vectors can be built performing an appropriate kinematic rotation on the H vectors that involve only $\mathbf{h}_2$ and $\mathbf{h}_3$ ones [13]. In this case, they can be written as:

$$\begin{aligned}
\mathbf{v_1} &= \mathbf{h_1},\\
\mathbf{v_2} &= \frac{1}{\sqrt{2}}(\mathbf{h}_2 - \mathbf{h}_3),\\
\mathbf{v_3} &= \frac{1}{\sqrt{2}}(\mathbf{h}_2 + \mathbf{h}_3).
\end{aligned} \tag{14}$$

Moreover, in similar form, the kinetic energy operator in the V scheme is given by

$$\hat{T}(\mathbf{v}) = -\frac{\hbar^2}{2m}\sum_{i=1}^{3}\nabla^2_{\mathbf{v}_i}, \tag{15}$$

and the relationships of the V vectors with the interparticle ones are

$$\begin{aligned}
\mathbf{r}_{12} &= 2\sqrt{2}\mathbf{v}_1,\\
\mathbf{r}_{13} &= \sqrt{2}\mathbf{v}_1 + (\sqrt{2}+1)\mathbf{v}_2 + (\sqrt{2}-1)\mathbf{v}_3,\\
\mathbf{r}_{14} &= \sqrt{2}\mathbf{v}_1 + (\sqrt{2}-1)\mathbf{v}_2 + (\sqrt{2}+1)\mathbf{v}_3,\\
\mathbf{r}_{23} &= -\sqrt{2}\mathbf{v}_1 + (\sqrt{2}+1)\mathbf{v}_2 + (\sqrt{2}-1)\mathbf{v}_3,\\
\mathbf{r}_{24} &= -\sqrt{2}\mathbf{v}_1 + (\sqrt{2}-1)\mathbf{v}_2 + (\sqrt{2}+1)\mathbf{v}_3,\\
\mathbf{r}_{34} &= 2(\mathbf{v}_3 - \mathbf{v}_2),
\end{aligned} \tag{16}$$

and $r_{ij} = |\mathbf{r}_{ij}|$.

As for the H and W schemes, six internal coordinates are defined for the V scheme. Figure 2 illustrates three distances v_1, v_2, and v_3, related to the modules of the vectors, and three angles ν_1, ν_2, and ν_3. If the z axis lies in the plane formed by $\mathbf{v}_2$ and $\mathbf{v}_3$ vectors, then ν_1 and ν_2 are directly the angles that orient the $\mathbf{v}_1$ with respect to the xyz axis. ν_3 is the angle between the $\mathbf{v}_2$ and $\mathbf{v}_3$ vectors.

Also, in this case, it can be introduced an hyperspherical parametrization to define the asymmetric hyperspherical coordinates as

$$\begin{aligned}
\rho &= \sqrt{|\mathbf{v}_1|^2 + |\mathbf{v}_2|^2 + |\mathbf{v}_3|^2},\\
\chi_6 &= \arctan \frac{|\mathbf{v}_1|}{\sqrt{|\mathbf{v}_2|^2 + |\mathbf{v}_3|^2}},\\
\chi_5 &= \arctan \frac{|\mathbf{v}_2|}{|\mathbf{v}_3|}.
\end{aligned} \tag{17}$$

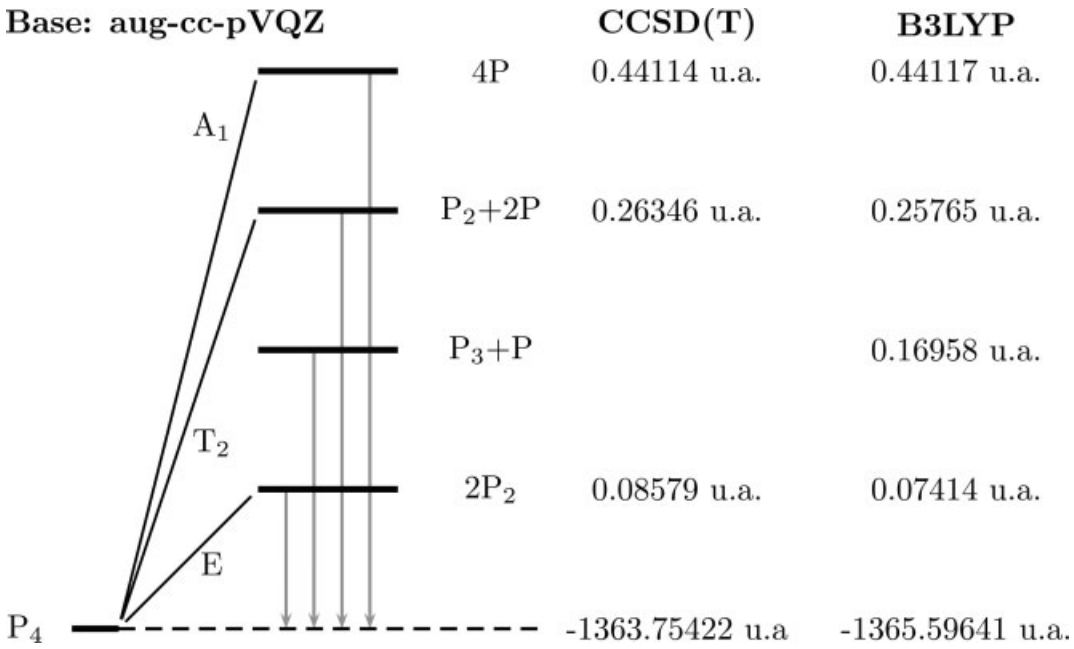

FIGURE 3. Energy diagram of the P_4 fragmentation. The energy given for the dissociation in $P_3 + P$ includes the relaxation of the spin.

These variables, as so as for the H and W schemes, are useful to represent the normal modes of vibration near the equilibrium configuration and to describe also large amplitude motions. The V scheme is used in section 3 to study the triplet electronic state of P_4.

Note that the definitions of the hyperradius ρ given in Eqs. (6), (12), and (17) are equivalents. In other words, ρ is an invariant of the schemes of local orthogonal coordinates, and it is related to the moment of inertia of the system [26].

3. Results and Discussions

Here, we discuss some geometric and energetic aspects of the P_4. The calculation of the electronic structures was performed using the Gaussian package [29]. The schemes of local orthogonal coordinates introduced previously are used here to describe the singlet and triplet P_4 molecules. In particular, the hyperradius and the hyperangles are associated to the vibrational modes in equilibrium configuration with the final scope of simplifying the representation of the internuclear potential. This approach can permit to solve the nuclear dynamics with a reduced basis set of functions.

3.1. STATE OF SINGLET

3.1.1. Structural and Energetic Properties

Following [6] we chose the aug-cc-pVQZ basis set to calculate the geometries and energies of the singlet P_4 and all the other molecules formally derived from its fragmentation, see Figure 3 and Table I. Two methodologies were used for the optimization of the equilibrium geometry of P_4 molecule. One is the coupled cluster method including single and double excitations plus triple excitations calculated with perturbation theory [CCSD(T)], whereas the other is the DFT procedure with the B3LYP functional. The calculations time were reduced imposing a tetrahedral configuration [4, 6–8], so only one degree of freedom was optimized. For CCSD(T) calculations, we have found an energy of -1363.75422 u.a. associated to the equilibrium distance of 2.2044 Å between every couple of phosphours. Similar results, -1365.59641 u.a. and 2.2079 Å, were obtained using the B3LYP method. For the equilibrium distance of the P_2, a value of 1.9054 Å was found by using the CCSD(T) method, while the obtained energy for the dissociation of the P_4 in $2P_2$ is of 53.83 kcal/mol (0.08579 u.a. or 225.2 kJ/mol). This energy is in agreement with the experimental values of 53.8 [31] and 53.7 kcal/mol [32]; it is also comparable to other theoretical values of the literature [6, 9, 10]. With the

TABLE I

Equilibrium geometries and energies calculated using the CCSD(T) and B3LYP methods and aug-cc-pVQZ basis set for P_n, $n = 1, \ldots, 4$.

Specie	Multiplicity	Method	Energy	Equilibrium distance(s)	Equilibrium angle
P	Doublet	CCSD(T)	−340.76798		
		B3LYP	−341.22848		
	Quadruplet	CCSD(T)	−340.82827		
		B3LYP	−341.28881		
P_2	Singlet	CCSD(T)	−681.83422	1.9054	
		B3LYP	−682.76113	1.8902	
		Exp. [30]		1.8934	
	Triplet	CCSD(T)	−681.74092	2.0846	
		B3LYP	−682.67383	2.0710	
P_3	Doublet	B3LYP	−1024.13801	2.1969	55.01
	Quadruplet	B3LYP	−1024.06259	2.1186	67.55
P_4	Singlet	CCSD(T)	−1363.75422	2.2044	
		B3LYP	−1365.59641	2.2079	
		Exp. [7]		2.1958	
			−1365.52767	$r_{13} = 2.2016$	$\theta_{312} = 59.03$
	Triplet	B3LYP		$r_{12} = 2.2643$	$\phi_{3124} = 108.22$

For the P_3 of doublet and quadruplet, we found isosceles configurations. The length of the two equal bonds and the apex angles are reported. Differently from the singlet P_4, the structure of the triplet P_4 belongs to the C_{2v} group of symmetry. Then, $r_{13} = r_{23} = r_{14} = r_{24}$ and consequently the four angles θ_{312}, θ_{321}, θ_{412}, and θ_{421} have the same value. Table also reports the dihedral angle ϕ_{3124} and the distance r_{12}. Energies are in u.a., distances in Å, and angles in degree.

B3LYP method, we have calculated the P_2 equilibrium distance of 1.8902 Å (approximately equal to that previewed by the CCSD(T) method) and the dissociation energy $P_4 \rightarrow 2P_2$ of 0.07414 u.a. This last value is 0.01165 u.a. less than that calculated with the CCSD(T). We have also used the CCSD(T) and B3LYP methodologies to calculate the energies involved in the fragmentation of the P_4 in $P_2 + 2P$ and 4P, whereas $P_3 + P$ has been calculated using only the B3LYP one, see Figure 3.

The optimization of the P_3 in the state of doublet gives as a result an isosceles structure, with two bond lengths of 2.1969 Å and apex bond angle of 55.01°, with an energy of −1024.13801 u.a. using the B3LYP procedure. This configuration can be compared with that of the P_3H molecule [5] where an hydrogen is added. The more stable multiplicity of the P atom (quadruplet) presents an energy of −341.28881 u.a. Therefore, the dissociation energy of the P_4 in $P_3 + P$, considering the relaxation of the spin, is of 0.16958 u.a.

The equilibrium distances and electronic energies can be explained in terms of hybridization. For example, neglecting the role of the d orbital, the phosphours in the P_4 molecules can be considered as having hybridization sp^3, whereas in the P_2 molecule the hybridization is sp. In the reaction $P_4 \rightarrow 2P_2$ the total number of chemical bonds is retained: the P_4 presents six σ bonds, whereas each P_2 presents one σ bond and two π bonds. As it is well known, the σ bonds are stronger than the π ones, and this implies that the reaction is endothermic. Obviously, the triple bond of the P_2 molecule is shorter than the single bonds of the P_4 molecule.

3.1.2. Analysis of the Normal Modes of Vibration

Considering the agreement of the results of P_4 molecule and its fragments using CCSD(T) and B3LYP methodologies, the calculation of normal modes of vibration of P_4 and the minimum energy path of P_4 dissociation in P_2 dimers are performed using the DFT method. This strategy allows the realization of this studies with a considerable reduction of computational time. In the Table II the frequencies of the normal modes of vibration of the singlet P_4, calculated at B3LYP/aug-cc-pVQZ level, are reported, jointly with the table of characters of the Td point group. The calculated frequencies are in agreement with the experimental ones reported in Ref. [33]. The associations of the normal modes of vibrations with the local orthogonal are done in the following.

TABLE II

Character table and normal modes of vibration of the singlet P_4 molecule calculated at B3LYP/aug-cc-pVQZ level of theory.

						Normal modes (cm^{-1})	
Td	E	$8C_3$	$3C_2$	$6S_4$	$6\sigma_d$	Present	Exp. [33]
A_1	1	1	1	1	1	616.349	600
A_2	1	1	1	−1	−1		
E	2	−1	2	0	0	368.523	361
T_1	3	0	−1	1	−1		
T_2	3	0	−1	−1	1	466.435	467

The lowest frequency of vibration, 368.5235 cm^{-1}, is double degenerate and belongs to the E irreducible representation. Analyzing the behavior of the two normal modes of vibration associated to these two frequencies, it was observed that they are represented by the coordinates χ_2 and δ_2 of the H scheme, see Figure 4. Because of the simplicity of this scheme, their behaviors are easily interpretable. The χ_2 coordinate, Figure 4(a), describes a particular stretching: when $\mathbf{h}_2$ increases, $\mathbf{h}_1$ and $\mathbf{h}_3$ decrease. The δ_2 angle is the dihedral angle of the scheme, Figure 4(b), and it describes a kind of torsional mode around the $\mathbf{h}_2$ vector. In this context, this vector can be interpreted as the average of the four bonds between the 1-3, 1-4, 2-3, and 2-4 phosphours. Another frequency of vibration is three time degenerate and belongs to the T_2 irreducible representation. Its value is 466.4347 cm^{-1}. Its modes of vibration are described by the χ_1 variable, Figure 4(c), and by the combinations of the δ_1 and δ_2 angles, showed in Figures 4(d) and (e). Note that, the δ_1 and δ_2 coordinates, as they are, do not belong to the T_2 irreducible representation, and

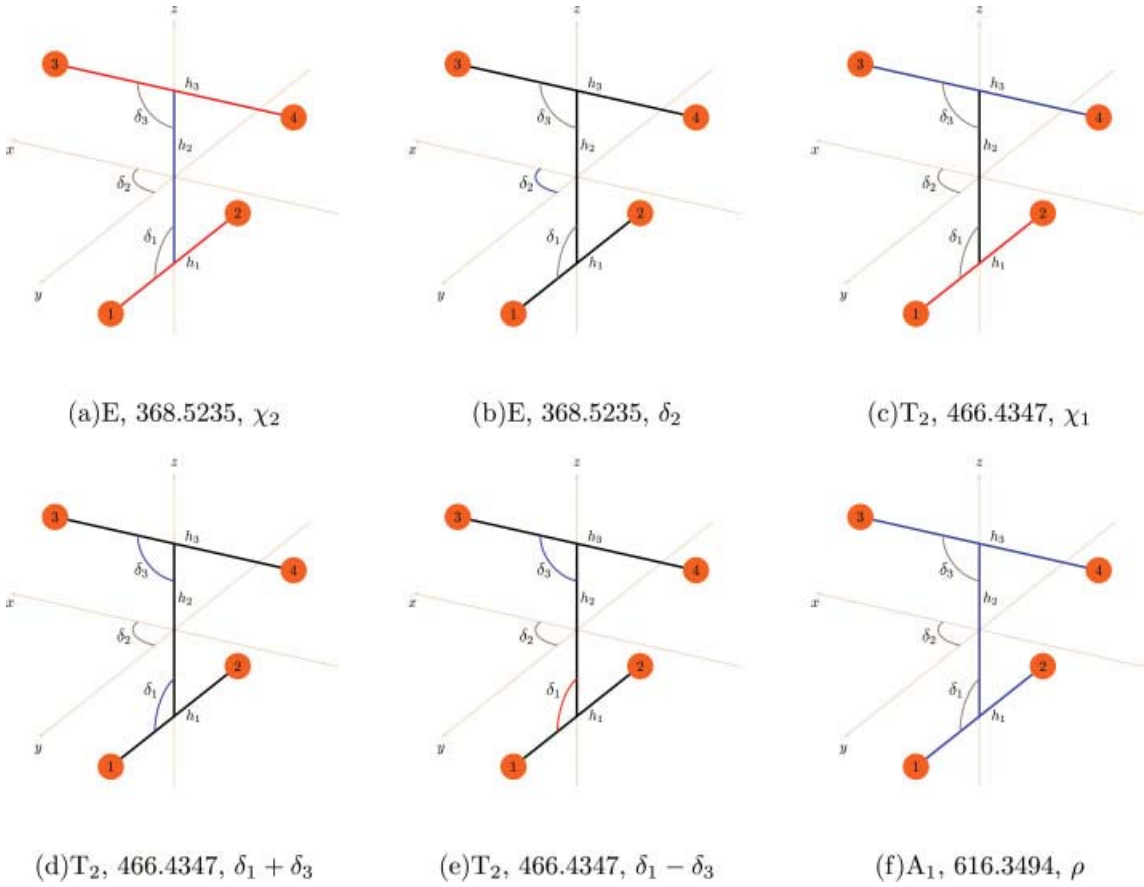

FIGURE 4. Interpretation of the modes of vibration using the H scheme and the hyperspherical variants. Irreducible representations, frequencies, and associated coordinates are given. The blue and red colors are used to indicate which coordinates of the H scheme are involved when an hyperspherical coordinate is varying: (a) Coordinate χ_2, when h_2 increases, h_1 and h_3 decrease. (b) Dihedral angle δ_2 between the vectors h_1 and h_3. (c) Coordinate χ_1, when h_1 increases, h_3 decreases. (d, e) Symmetric ($\delta_1 + \delta_2$) and asymmetric ($\delta_1 - \delta_2$) bendings, respectively. (f) Hyperradius ρ, symmetric stretching. [Color figure can be viewed in the online issue, which is available at wileyonlinelibrary.com.]

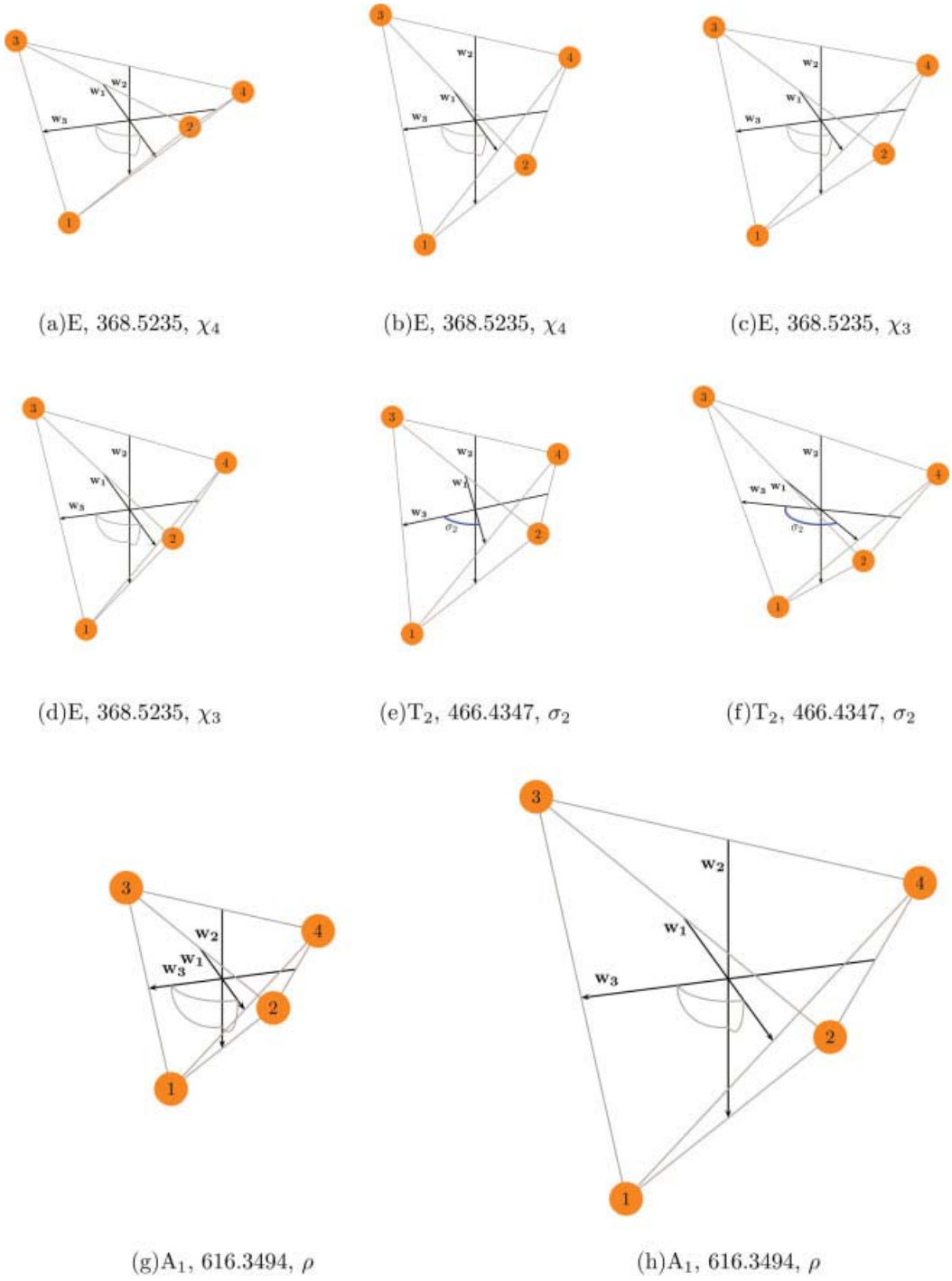

FIGURE 5. Interpretation of the modes of vibration using the W scheme. Irreducible representations, frequencies, and associated coordinates are given. Figures 5(a) and (b) present the configuration that the atoms assume for small and big values of χ_4, when the other coordinates are fixed to their values at the equilibrium. Figures 5(c) and (d) are identical to the first two, but they are related to the variable χ_3. Figures 5(e) and (f) show the displacement of the phosphours in function of σ_2 when the other variables are fixed to their values at the equilibrium. In particular, for small (big) values of σ_2 the distance between particles 3 and 4 is smaller (bigger) than the equilibrium one. The behavior of particles 1 and 2 is opposite to that of 3 and 4 when σ_2 varies. Moreover, this coordinate retains the C_{2v} symmetry. Figures 5(g) and (h) show the molecule for small and big values of ρ. [Color figure can be viewed in the online issue, which is available at wileyonlinelibrary.com.]

the introduction of the W scheme is important to improve the description of regular tetrahedral systems like P_4. As discussed above, χ_2 coincides with χ_4, see Figures 5(a) and (b), while the δ_2 variable can be replaced by the χ_3 coordinate, see Figures 5(c) and (d). In addition, the symmetrization introduced to build the W scheme leads to three variables, the σ_i ($i = 1, 2, 3$) angles, that have the same behavior, only permuting the numeration of the particles. For example, in Figures 5(e) and (f), the configurations for small and big values of σ_2 are shown, respectively. It was found that these angles describe the modes of vibration associated to the T_2 representation. The last frequency is not degenerate and belongs to the A_1 irreducible representation. Its value is of 616.3494 cm^{-1} and is associated with the symmetric stretching described by the variable ρ, common to the H and W schemes, see Figures 4(e), 5(g) and (h). This variable is found to be near separable specially in the region around the minimum of the potential energy surface.

Resuming, the H scheme is basic and more intuitive, but a correct representation of the symmetries of the modes of vibration can be obtained with the hyperspherical coordinates derived from the W scheme. Curiously, the hyperradius, common to the two schemes, is associated to the biggest frequency of vibration, while χ_2, or equivalently χ_4, describes the mode of vibration with the lowest frequency.

It is known that the normal modes of vibration obtained by diagonalization of the Hessian matrix, because of their linearity, are a good set of coordinates only for small deviation from the equilibrium configuration. On the other hand, the hyperspherical coordinates follow the modes of vibration also for large amplitude of the variables. Moreover, the hyperradius and one hyperangle can sometimes describe a reaction channel. For the singlet P_4, it is found that the dissociation channels in $2P_2$, $P_2 + 2P$, and 4P retain particular symmetries of the Td point group. In particular, the dissociation channel in 4P behaves like the irreducible representation A_1 and can be followed with the ρ variable (Fig. 3). The six $P_2 + 2P$ dissociation channels behave as the T_2 representation and can be followed near the equilibrium by the three angles σ_i ($i = 1, 2, 3$), see Figure 5. For the complete description of the channels, the hyperradius must also be considered. We show in the next as the χ_3 and χ_4 coordinates, that belong to the E irreducible representation, plus the ρ variable describe the three dissociation channels in $2P_2$. In addition, particular combinations of the two hyperangles permit to describe the system in the three square configurations. The dissociation in $P_3 + P$ cannot be obtained following a mode of vibration of the singlet state of P_4, but exciting this molecule to the triplet state, the nature of the vibrations changes and the fragmentation in P_3 is favored, as can be seen in Section 3.2.

3.1.3. Dissociation in $2P_2$

As it was observed, the vibration that leads to one of the dissociation channels in $2P_2$ can be followed with the coordinates χ_2 (H scheme) or χ_4 (W scheme). Anyway, we use χ_4 to discuss our results because the behavior of the other coordinates of the Wigner scheme is more efficient. It was found that the three angles σ_i remain fixed to their value at the equilibrium ($\pi/2$). Also, χ_3 does not vary and remain fixed to $\pi/4$. More exactly, this coordinate follows the other channels of dissociation in $2P_2$. For small deviation from the equilibrium value of the χ_4 variable, also ρ is approximately constant, but it necessarily increases when the coordinate χ_4 assume values significantly distant from that of the equilibrium. The characteristic points and the P_4 dissociation channels are displayed in Figure 6.

Figure 6(a) shows some particular configurations in function of the coordinates χ_3 and χ_4 when the angles σ_i ($i = 1, 2, 3$) are fixed to their value at the equilibrium ($\pi/2$) and the hyperradius ρ may take any value between zero and infinity. Starting from the back point, regular tetrahedral configuration, each reactive (dissociative) channel in $2P_2$ is shown. In particular, three couples of phosphours (12:34, 13:24, and 14:23) are possible with various relative orientations. Keeping χ_3 fixed to $\pi/4$ and increasing the coordinate χ_4 from zero to $\pi/2$—continuous blue line in Figure 6(a)—we follow the path that transforms the system from a square configuration to that indicated by the cyan point with coordinate ($2\pi/5$, $\pi/4$). In this configuration, phosphours 12 and 34 are outlined as shown in Figure 5(b). The other two cyan points indicate equivalent configurations, where the phosphours are permuted. For $\chi_4 > 0$ and different from that of the equilibrium, the relative orientation of the two diatoms 12 and 34 implies that the described configurations belong to the S_4 point group. $\chi_4 = \pi/2$ corresponds to the collapse of the phosphours 1 with 2 and 3 with 4 (yellow line). Other nonphysical points [represented in yellow in Fig. 6(a)] are for $\chi_4 = 0$ when χ_3 is zero or $\pi/2$. Magenta points are representative of the

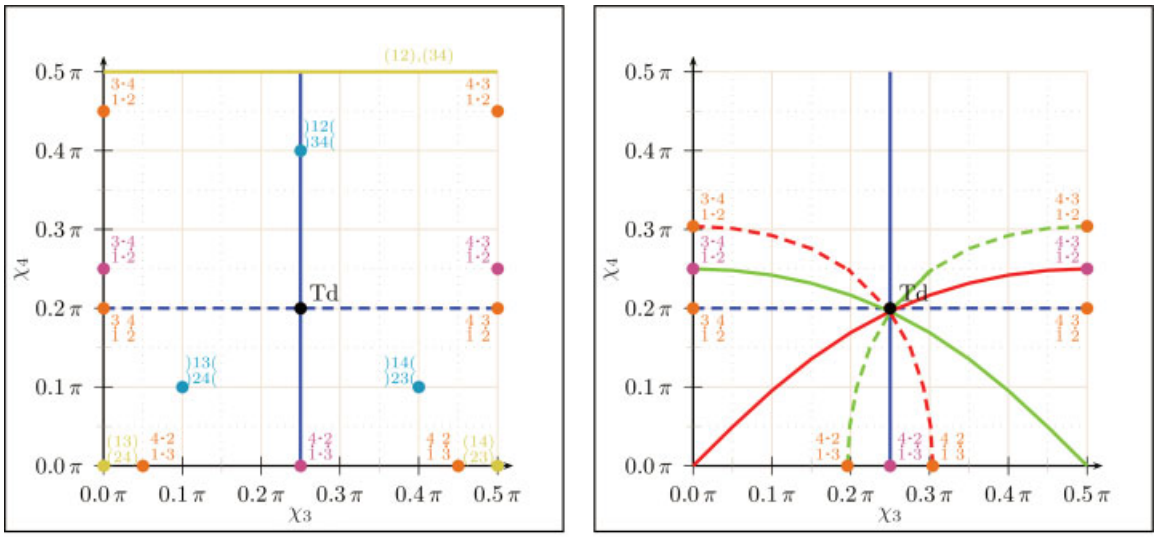

FIGURE 6. Channels of dissociation of the P_4 in $2P_2$ in function of χ_3 and χ_4 coordinates. The black point indicates the regular tetrahedral configuration. Continuous blue line follows the χ_4 coordinate from zero, square configuration, to a value near to $\pi/2$, that corresponds to the perpendicular configuration, see Figure 5(b). These and the other square and perpendicular configurations are indicated with magenta and cyan points, respectively. Dashed blue line follows the coordinate χ_3 and connects two rectangular configurations (brown points). These configurations are related to the dissociation channels in $2P_2$ with all the phosphours in the same plane. Yellow points represent nonphysical configurations (nucleus superposed). Red and green lines are equivalent to the blue ones when a permutation of the nucleus is performed. [Color figure can be viewed in the online issue, which is available at wileyonlinelibrary.com.]

square configurations, whereas brown points indicate for which values of the variables χ_3 and χ_4 the planar dissociations in $2P_2$ are obtained. Note that each configuration determined by values of χ_3 and χ_4 simultaneously different from zero and $\pi/2$ is classically chiral, and the relative enantiomer is obtained varying one of the angles σ by π. In Figure 6(b), solid red and green lines show two paths equivalent to that described by the blue one. These lines describe identical configuration where the order of the phosphours is permuted. Analogously, also the dashed lines represent equivalent paths, but the limit configurations are planar and nonchiral.

Figures 7 and 8 map the behavior of an exit channel in function of h_2 when $h_1 = h_3$. In Figure 7 two principal areas are distinguishable. The smallest one, with small values of h_2, is the region near the equilibrium (tetrahedral) configuration. The minimum energy path of the vibration described by χ_4 is shown with a black line that starts from the equilibrium configuration, on the left, and stops for a value of h_2 equal to 2.55 Å, see Figure 8. For this value of h_2 the surface inverts the concavity. This can be explained in terms of the hybridization that is sp^3 in the first area (that of the P_4) and sp in the second one. This second area describes the potential of the two diatoms P_2, and also in this case the minimum energy path is shown with a black line. In particular, Figure 7 shows that the equilibrium bond lengths of the two diatoms h_1 ($= h_3$) in function of h_2 substantially do not vary until that the triple bonds are destruct and the hybridization changes from sp to sp^3.

3.1.4. Representation of the Potential Energy Surface

From the discussion about the relation between the hyperspherical coordinates of the W scheme and normal modes of vibration, the potential energy surface of the singlet P_4 near of the equilibrium can be fitted with a expansion in hyperspherical coordinates within the spiritus of the "many body expansion" as follows:

$$V = V_0 + V_1(\rho) + V_2(\chi_3) + V_3(\chi_4) + V_4(\sigma_1) + V_4(\sigma_2) + V_4(\sigma_3) + V_c, \quad (18)$$

where $V = 0$ is the energy of the P_4 in the equilibrium configuration, V_i ($i = 1, 2, 3, 4$) are the potential

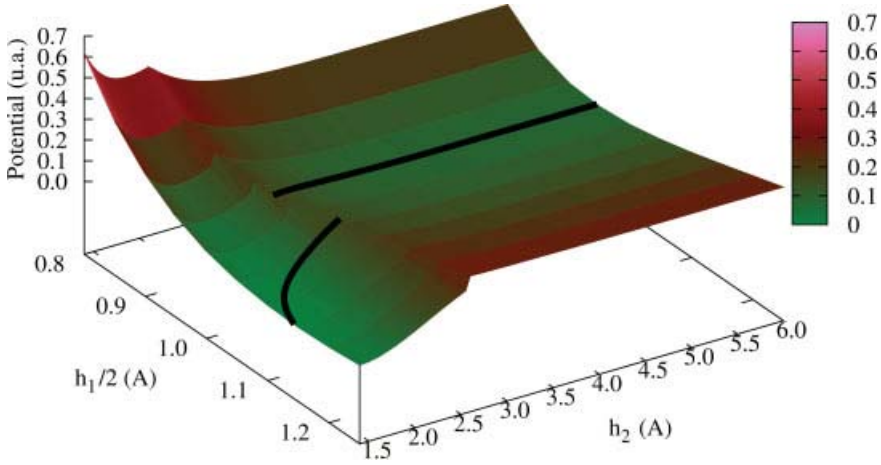

FIGURE 7. Bidimentional profile of the dissociation of the P_4 in $2P_2$ calculated at B3LYP/aug-cc-pVQZ level of theory. The variable χ_3 is fixed to $\pi/2$, so $h_1 = h_3$. Red points: DFT values. Black lines: MEP of the dissociation. Note that the MEP has a discontinuity in the region where the hybridization of the four phosphours changes from sp^3 (P_4 molecule) to sp (P_2 molecule). [Color figure can be viewed in the online issue, which is available at wileyonlinelibrary.com.]

functions that fit the energies along the six internal coordinates, while V_c is a corrective potential that describes the coupling of the potential and depends all the internal coordinates. The three functions that describe the potential along the σ_i hyperangles need to have the same functional form. Each term of the potential, except V_0, needs to have an appropriate shape and adaptable coefficients to fit the ab initio points.

3.2. STATE OF TRIPLET

The triplet P_4 is formally obtained exciting one electron of the singlet P_4 from a bond orbital to an antibond one. It results in a new equilibrium configuration of P_4 where one P–P bond is weaker than the same bond in the singlet P_4. Consequently, the tetrahedral geometry is lost, and the equilibrium configuration of the triplet state of P_4, as expected, belongs to the C_{2v} symmetry, see Figure 2 and Table III. In particular, the calculation at B3LYP level of theory using the aug-cc-pVQZ basis set gives an energy of −1365.52767 u.a., while the internuclear distances r_{ij} are as follows: $r_{13} = r_{23} = r_{24} = r_{14} = 2.20$ Å, $r_{12} = 2.26$ Å, and $r_{34} = 3.06$ Å. The normal modes of vibration are found to be drastically different from those of the singlet state. Consequently, the set of coordinates necessary to describe the triplet needs to

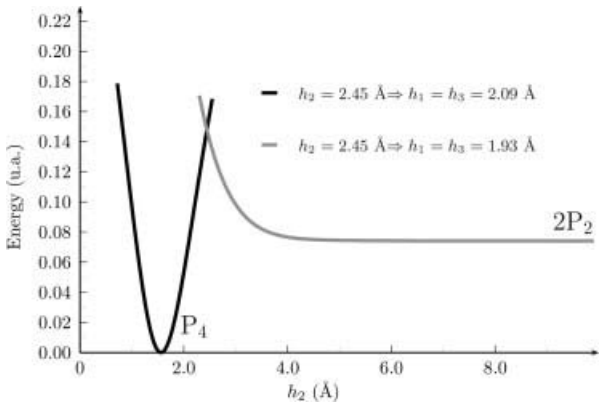

FIGURE 8. MEP of the dissociation of the P_4 in $2P_2$ along the coordinate h_2, $h_1 = h_3$.

TABLE III

Normal modes of vibration of the triplet P_4 molecule, calculated at B3LYP/aug-cc-pVQZ level of theory.

Normal modes (cm^{-1})	Coordinate	Irreducible representation
236.820	ν_3	A
314.045	ν_2	A
349.469	χ_6	A
402.293	ν_1	B
461.922	χ_5	B
549.977	ρ	A

Associated coordinates and irreducible representation (C_{2v} group) are given.

be changed to one that belongs to the C_{2v} symmetry. It is suggested that the V scheme has the appropriate symmetries and describe well the normal modes of vibration of triplet P_4.

In Table III the frequencies of the normal modes of vibration calculated at B3LYP/aug-cc-pVQZ level are associated with the V hyperspherical coordinates and with the irreducible representation of the C_{2v} group of symmetry. Also here, the hyperradius ρ given in Eq. (6) describes the dissociation of the P_4 in 4P; ν_3 follows the elliptical vibration of the atoms 3 and 4 on a plane perpendicular to the vector $\mathbf{v}_1$, and it is related to the lowest mode of vibration; ν_2 is related to the rotation of the diatom 1-2 around the z axis, and for big positive or negative variation of this angle the configuration limits (1-3), (2-4) and (1-4), (2-3) can be obtained; χ_6 follows the dissociative channels that lead to $2P + P_2$ systems; and ν_1 and χ_5 are related to the dissociation in triangular and linear P_3, respectively.

4. Conclusion and Remarks

Hyperspherical variants of the H, W, and V orthogonal schemes were presented and discussed with particular attention to the behavior of the P_4 system under a variation of the internal coordinates. Geometrical and energetic properties of the P_4 molecule in singlet and triplet states were calculated using CCSD(T) and DFT methods. We also describe the vibrational modes of singlet and triplet P_4 with appropriate schemes of local orthogonal coordinates. In particular, the vibrational modes of the singlet state of P_4 were investigated to describe the reactivity of the P_4 and its fragmentation channels. We found that these coordinates are appropriated to the description of the dissociative channels, permitting a simple representation of the globally potential energy surface of the P_4 molecule. In particular, we verified that W scheme improves the description of regular tetrahedral systems like the singlet P_4.

Moreover, we inferred that these coordinates can permit the reduction of the number of ab initio points necessary to build up a satisfactory potential energy surface. This is because the appropriated coordinates factorize the interaction potential. Therefore, it should be necessary to calculate the PES value principally along the vibrational modes and reaction paths. In addition, all these configurations can be successfully provided by the local orthogonal coordinates [3, 26].

The Wigner scheme introduces the symmetrization of the H one to treat four identical particles in the space-fixed reference frame. The introduction of the three Euler angles permits to treat the system in the body-fixed reference frame. As it is well known, two of these angles vary between zero and 2π, whereas the third has a range of π. The internal coordinates ρ, χ_3, and χ_4 were calculated starting from the modules of the W vectors that take values greater than or equal to zero. This choice for the Euler angles and for the length of the vectors implies that one of the internal angles σ has a range of 2π, whereas the other two have a range of π. This asymmetry can be handled without problem, or it may be easily removed by extending the range of the length of the W vectors. A more detailed discussion may be done in the future.

The local orthogonal coordinates and the hyperspherical variants described in this article can be applied, in future works, to the study of other tetratomic systems with tetrahedral dominated equilibrium configuration. Some examples are Be_4, Mg_4 [34], and N_4 [35]. These systems are particularly reactive, so the description of their global potential energy surfaces could be greatly improved from the use of hyperspherical coordinates that well describe the modes of vibration as so as the dissociative channels. Another interesting perspective is to extend the hyperspherical parameterizations for the description of clusters of phosphours and others atoms, such as silicon [36, 37], aluminum [38], and selenium [39].

Appendix: Generalized W Scheme for Unequal Masses

The Wigner scheme is defined only for systems of four particles with identical masses. In this appendix, we propose a possible generalization for systems like P_4 where one or more atoms are substituted with isotopes or other atoms. Moreover, the scheme of coordinates presented here is obtained through a particular scaling of the vectors that can be explored for the treatment of systems like the H_2. In fact, this molecule has four particles, two protons and two electrons. Although the V scheme can describe with success the ionization channel ($H_2 \rightarrow H_2^+ + e^-$), the modified Wigner scheme has the opportune symmetries to treat the bound system. Observe that the interaction potential between each couple of particles is of coulombian type. In other words, the potential between the four particles is symmetric or

(due to the charge) antisymmetric with respect to the interchange of two particles.

At this level, it is important to remember the principal characteristics of an orthogonal set of coordinates. First, each internal coordinate needs to describe a particular vibration mode, or, equivalently, the interaction potential needs to be approximatively factorized when described in the chosen coordinates. Second, the kinetic operator cannot present cross-derivative terms.

To extend the Wigner scheme for the general case of unequal masses (observing the above rules on the coordinates), we introduce an opportune mass scaling on the position vectors $\mathbf{r}_i$. To illustrate this scaling, we use the H_2 molecule. Its kinetic energy operator is as follows:

$$\hat{T}(\mathbf{r}) = -\frac{\hbar^2}{2m_\mathrm{p}}\nabla^2_{r_{1\mathrm{p}}} - \frac{\hbar^2}{2m_\mathrm{p}}\nabla^2_{r_{2\mathrm{p}}} - \frac{\hbar^2}{2m_\mathrm{e}}\nabla^2_{r_{1\mathrm{e}}} - \frac{\hbar^2}{2m_\mathrm{e}}\nabla^2_{r_{2\mathrm{e}}}, \tag{A1}$$

where m_p and m_e are the masses of the protons and electrons, respectively. $\mathbf{r}_{1\mathrm{p}}$ and $\mathbf{r}_{2\mathrm{p}}$ are the position vectors of the two protons. Analogously, $\mathbf{r}_{1\mathrm{e}}$ and $\mathbf{r}_{2\mathrm{e}}$ are the position vectors of the two electrons. In spherical coordinates, each vector $\mathbf{r}$ is written in terms of its module $r = |\mathbf{r}|$ and two angles ϑ and φ. So, the kinetic operator of one electron is

$$\hat{T}(\mathbf{r}_{1\mathrm{e}}) = -\frac{\hbar^2}{2m_\mathrm{e}}\left[\frac{1}{r^2_{1\mathrm{e}}}\frac{\partial}{\partial r_{1\mathrm{e}}}r^2_{1\mathrm{e}}\frac{\partial}{\partial r_{1\mathrm{e}}} + \frac{1}{r^2_{1\mathrm{e}}}\Upsilon_{1\mathrm{e}}\right],$$
$$\Upsilon_{1\mathrm{e}} = \frac{1}{\sin\vartheta_{1\mathrm{e}}}\frac{\partial}{\partial\vartheta_{1\mathrm{e}}}\sin\vartheta_{1\mathrm{e}}\frac{\partial}{\partial\vartheta_{1\mathrm{e}}} + \frac{1}{\sin^2\vartheta_{1\mathrm{e}}}\frac{\partial^2}{\partial\varphi^2_{1\mathrm{e}}}. \tag{A2}$$

Let us define a mass-scaled module of the position vector as follows:

$$\varrho_{1\mathrm{e}} = \sqrt{\frac{m_\mathrm{e}}{m_\mathrm{p}}}\, r_{1\mathrm{e}}. \tag{A3}$$

So,

$$\frac{\partial}{\partial r_{1\mathrm{e}}} = \sqrt{\frac{m_\mathrm{e}}{m_\mathrm{p}}}\frac{\partial}{\partial\varrho_{1\mathrm{e}}}, \tag{A4}$$

and

$$\hat{T}(\varrho_{1\mathrm{e}}) = -\frac{\hbar^2}{2m_\mathrm{p}}\left[\frac{1}{\varrho^2_{1\mathrm{e}}}\frac{\partial}{\partial\varrho_{1\mathrm{e}}}\varrho^2_{1\mathrm{e}}\frac{\partial}{\partial\varrho_{1\mathrm{e}}} + \frac{1}{\varrho^2_{1\mathrm{e}}}\Upsilon_{\varrho_{1\mathrm{e}}}\right]. \tag{A5}$$

The kinetic energy operator of Eq. (A1) is transformed in:

$$\hat{T} = -\frac{\hbar^2}{2m_\mathrm{p}}\left(\nabla^2_{r_{1\mathrm{p}}} + \nabla^2_{r_{2\mathrm{p}}} + \nabla^2_{\varrho_{1\mathrm{e}}} + \nabla^2_{\varrho_{2\mathrm{e}}}\right), \tag{A6}$$

and the generalized Wigner scheme (GWS) can be build.

The vectors of the GWS are as follows:

$$\begin{aligned}
\mathbf{w}_1 &= (\mathbf{r}_{1\mathrm{p}} - \mathbf{r}_{2\mathrm{p}} - \boldsymbol{\varrho}_{1\mathrm{e}} + \boldsymbol{\varrho}_{2\mathrm{e}})/4,\\
\mathbf{w}_2 &= (\mathbf{r}_{1\mathrm{p}} + \mathbf{r}_{2\mathrm{p}} - \boldsymbol{\varrho}_{1\mathrm{e}} - \boldsymbol{\varrho}_{2\mathrm{e}})/4,\\
\mathbf{w}_3 &= (\mathbf{r}_{1\mathrm{p}} - \mathbf{r}_{2\mathrm{p}} + \boldsymbol{\varrho}_{1\mathrm{e}} - \boldsymbol{\varrho}_{2\mathrm{e}})/4,\\
\mathbf{w}_4 &= (\mathbf{r}_{1\mathrm{p}} + \mathbf{r}_{2\mathrm{p}} + \boldsymbol{\varrho}_{1\mathrm{e}} + \boldsymbol{\varrho}_{2\mathrm{e}})/4.
\end{aligned} \tag{A7}$$

Note that $\mathbf{w}_4$ is not the vector of the center of mass and the 12-dimensional problem must be affronted. This is the price to be paid to use the GWS. The inverses are as follows:

$$\begin{aligned}
\mathbf{r}_{1\mathrm{p}} &= +\mathbf{w}_1 + \mathbf{w}_2 + \mathbf{w}_3 + \mathbf{w}_4,\\
\mathbf{r}_{2\mathrm{p}} &= -\mathbf{w}_1 + \mathbf{w}_2 - \mathbf{w}_3 + \mathbf{w}_4,\\
\boldsymbol{\varrho}_{1\mathrm{e}} &= -\mathbf{w}_1 - \mathbf{w}_2 + \mathbf{w}_3 + \mathbf{w}_4,\\
\boldsymbol{\varrho}_{2\mathrm{e}} &= +\mathbf{w}_1 - \mathbf{w}_2 - \mathbf{w}_3 + \mathbf{w}_4,
\end{aligned} \tag{A8}$$

also

$$\begin{aligned}
\mathbf{r}_{1\mathrm{e}} &= \sqrt{\frac{m_\mathrm{p}}{m_\mathrm{e}}}\,\boldsymbol{\varrho}_{1\mathrm{e}},\\
\mathbf{r}_{2\mathrm{e}} &= \sqrt{\frac{m_\mathrm{p}}{m_\mathrm{e}}}\,\boldsymbol{\varrho}_{2\mathrm{e}}.
\end{aligned} \tag{A9}$$

The kinetic operator is simply:

$$\hat{T}(\mathbf{w}) = -\frac{\hbar^2}{8m_\mathrm{p}}\sum_{i=1}^{4}\nabla^2_{\mathbf{w}_i}, \tag{A10}$$

while the distances between the particles are calculated using:

$$\begin{aligned}
\mathbf{r}_{2\mathrm{p},1\mathrm{p}} &= \mathbf{r}_{1\mathrm{p}} - \mathbf{r}_{2\mathrm{p}} = 2(\mathbf{w}_1 + \mathbf{w}_3),\\
\mathbf{r}_{1\mathrm{e},1\mathrm{p}} &= \mathbf{r}_{1\mathrm{p}} - \mathbf{r}_{1\mathrm{e}} = \left(1 + \sqrt{\frac{m_\mathrm{p}}{m_\mathrm{e}}}\right)(\mathbf{w}_1 + \mathbf{w}_2)\\
&\quad + \left(1 - \sqrt{\frac{m_\mathrm{p}}{m_\mathrm{e}}}\right)(\mathbf{w}_3 + \mathbf{w}_4),
\end{aligned}$$

$$\mathbf{r}_{2e,1p} = \mathbf{r}_{1p} - \mathbf{r}_{2e} = \left(1 + \sqrt{\frac{m_p}{m_e}}\right)(\mathbf{w}_2 + \mathbf{w}_3) + \left(1 - \sqrt{\frac{m_p}{m_e}}\right)(\mathbf{w}_1 + \mathbf{w}_4),$$

$$\mathbf{r}_{1e,2p} = \mathbf{r}_{2p} - \mathbf{r}_{1e} = \left(1 + \sqrt{\frac{m_p}{m_e}}\right)(\mathbf{w}_2 - \mathbf{w}_3) + \left(1 - \sqrt{\frac{m_p}{m_e}}\right)(\mathbf{w}_4 - \mathbf{w}_1),$$

$$\mathbf{r}_{2e,2p} = \mathbf{r}_{2p} - \mathbf{r}_{2e} = \left(1 + \sqrt{\frac{m_p}{m_e}}\right)(\mathbf{w}_2 - \mathbf{w}_1) + \left(1 - \sqrt{\frac{m_p}{m_e}}\right)(\mathbf{w}_4 - \mathbf{w}_3),$$

$$\mathbf{r}_{2e,1e} = \mathbf{r}_{1e} - \mathbf{r}_{2e} = 2\sqrt{\frac{m_p}{m_e}}(\mathbf{w}_3 - \mathbf{w}_1). \qquad \text{(A11)}$$

ACKNOWLEDGMENTS

The electronic structure calculations were executed on the cluster "Prometeu" of the Institute of Physics - UFBA. The authors are grateful to Professor Vincenzo Aquilanti for the interesting discussions about the Wigner scheme.

References

1. Hirschfelder, J. O.; Dahler, J. S. Proc Natl Acad Sci USA 1956, 42, 363.
2. Jepsen, D. W.; Hirschfelder, J. O. Proc Natl Acad Sci USA 1959, 45, 249.
3. Maciel, G. S.; Bitencourt, A. C. P.; Ragni, M.; Aquilanti, V. Chem Phys Lett 2006, 432, 383.
4. Novaro, O.; Castillo, S. Int J Quantum Chem 1984, 26, 411.
5. Glukhovtsev, M. N.; Bach, R. D.; Laiter, S. Int J Quantum Chem 1997, 62, 373.
6. Persson, B. J.; Taylor, R.; Lee., T. J. J Chem Phys 1997, 107, 5051.
7. Boudon, V.; Mkadmi, E. B.; Bürger, H.; Pierre, G. Chem Phys Lett 1999, 305, 21.
8. Hohm, U. Chem Phys Lett 1999, 311, 117.
9. Wang, D.; Xiao, C.; Xu, W. J Mol Struct 2006, 759, 225.
10. Haser, M.; Treutler, O. J Chem Phys 1994, 102, 3703.
11. Yao, S.; Xiong, Y.; Milsmann, C.; Bill, E.; Pfirrmann, S.; Limberg, C.; Driess, M. Chem Eur J 2010, 16, 436.
12. Su, Y.-N.; Chu, S.-Y. Int J Quantum Chem 1995, 54, 43.
13. Ragni, M.; Bitencourt, A. C. P.; Aquilanti, V. Int J Quantum Chem 2007, 107, 2870.
14. Yu, H.-G.; Muckerman, J. T. J Mol Spectrosc 2002, 214, 11.
15. Mladenovic, M. J Chem Phys 2000, 112, 1070.
16. Kozin, I. N.; Lawa, M. M.; Tennyson, J.; Hutson, J. M. Comput Phys Commun 2004, 163, 117.
17. Aquilanti, V.; Bartolomei, M.; Carmona-Novillo, E.; Pirani, F. J Chem Phys 2003, 118, 2214.
18. Carmona-Novillo, E.; Pirani, F.; Aquilanti, V. Int J Quantum Chem 2004, 99, 616.
19. Kozina, I. N.; Law, M. M.; Tennyson, J.; Hutson, J. M. J Chem Phys 2005, 122, 064309.
20. Bitencourt, A. C. P.; Ragni, M.; Maciel, G. S.; Aquilanti, V.; Prudente, F. V. J Chem Phys 2008, 129, 154316.
21. Aquilanti, V.; Ascenzi, D.; Bartolomei, M.; Cappelletti, D.; Cavalli, S.; de de Castro Vitores, M.; Pirani, F. J Am Chem Soc 1999, 121, 10794.
22. Aquilanti, V.; Bartolomei, M.; Cappelletti, D.; Carmona-Novillo, E.; Pirani, F. J Chem Phys 2002, 117, 615.
23. Aquilanti, V.; Bartolomei, M.; Cappelletti, D.; Carmona-Novillo, E.; Pirani, F. Phys Chem Chem Phys 2001, 3, 3891.
24. Aquilanti, V.; Carmona-Novilloa, E.; Pirani, F. Phys Chem Chem Phys 2002, 4, 4970.
25. Aquilanti, V.; Cavalli, S. J Chem Soc Faraday Trans 1997, 93, 801.
26. Ragni, M.; Lombardi, A.; Barreto, P. R. P.; Bitencourt, A. C. P. J Phys Chem A 2009, 113, 15355.
27. Hirschfelder, J. O. Annu Rev Phys Chem 1983, 34, 1.
28. Aquilanti, V.; Cavalli, S. J Chem Phys 1986, 85, 1355.
29. Frisch, M. J.; Trucks, G. W.; Schlegel, H. B.; Scuseria, G. E.; Robb, M. A.; Cheeseman, J. R.; Montgomery, J. A.; Vreven, J. T.; Kudin, K. N.; Burant, J. C.; Millam, J. M.; Iyengar, S. S.; Tomasi, J.; Barone, V.; Mennucci, B.; Cossi, M.; Scalmani, G.; Rega, N.; Petersson, G. A.; Nakatsuji, H.; Hada, M.; Ehara, M.; Toyota, K.; Fukuda, R.; Hasegawa, J.; Ishida, M.; Nakajima, T.; Honda, Y.; Kitao, O.; Nakai, H.; Klene, M.; Li, X.; Knox, J. E.; Hratchian, H. P.; Cross, J. B.; Bakken, V.; Adamo, C.; Jaramillo, J.; Gomperts, R.; Stratmann, R. E.; Stratmann, R. E.; Yazyev, O.; Austin, A. J.; Cammi, R.; Pomelli, C.; Ochterski, J. W.; Ayala, P. Y.; Morokuma, K.; Voth, G. A.; Salvador, P.; Dannenberg, J. J.; Zakrzewski, V. G.; Dapprich, S.; Daniels, A. D.; Strain, M. C.; Farkas, O.; Malick, D. K.; Rabuck, A. D.; Raghavachari, K.; Foresman, J. B.; Ortiz, J. V.; Cui, Q.; Baboul, A. G.; Clifford, S.; Cioslowski, J.; Stefanov, B. B.; Liu, G.; Liashenko, A.; Piskorz, P.; Komaromi, I.; Martin, R. L.; Fox, D. J.; Keith, T.; Al-Laham, M. A.; Peng, C. Y.; Nanayakkara, A.; Challacombe, M.; Gill, P. M. W.; Johnson, B.; Chen, W.; Wong, M. W.; Gonzalez, C.; Pople, J. A. Gaussian 03, Revision C.02; Gaussian, Inc.: Wallingford, CT, 2004.
30. Huber, K. P.; Herzberg, G. Molecular Spectra and Molecular Structure, Vol. 4: Constants of Diatomic Molecules; Van Nostrand: New York, 1979.
31. CODATA. J Chem Thermodyn 1978, 10, 903.
32. Chase, M. W.; Davies, C. A.; Downey, J. R.; Frurip, D. J.; Donald, R. A. M.; Syverud, A. N. JANAF Thermochemical Tables, 3rd ed.; American Chemical Society: Washington, DC, 1985.
33. Edwards, H. G. M. J Mol Struct 1993, 295, 95.
34. Díaz, C. C.; Kaplan, I. G.; Roszak, S. J Mol Model 2005, 11, 330.
35. Xenides, D. J Mol Struct: THEOCHEM 2007, 804, 41.
36. Yang, J.; Xu, W.; Xiao, W. J Mol Struct: THEOCHEM 2005, 719, 89.
37. Li, C.; Yang, J.; Bai, X. J Mol Struct: THEOCHEM 2005, 755, 65.
38. Guo, L.; Wu, S. H.; Jin, Z. H. Int J Mass Spectrom 2005, 240, 149.
39. Xu, W.; Bai, W. J Mol Struct: THEOCHEM 2008, 854, 89.